Journal of Materials Chemistry B

PAPER



Cite this: J. Mater. Chem. B, 2017, 5, 3217

# Hybrid supramolecular gels of Fmoc-F/halloysite nanotubes: systems for sustained release of camptothecin†‡

C. Rizzo,[a] R. Arrigo,[b] F. D'Anna,*[a] F. Di Blasi,[c] N. T. Dintcheva,[b] G. Lazzara,[d] F. Parisi,[d] S. Riela,*[a] G. Spinelli[c] and M. Massaro[a]

Received 27th January 2017,
Accepted 30th March 2017

DOI: 10.1039/c7tb00297a

rsc.li/materials-b

Supramolecular gel hybrids obtained by self-assembly of Fmoc-L-phenylalanine (Fmoc-F) in the presence of functionalized halloysite nanotubes (f-HNT) were obtained in biocompatible solvents and employed as carriers for the delivery of camptothecin (CPT) molecules. The synthesis of the new f-HNT material as well as its characterization are described. The properties of the hybrid hydrogels and organogels were analyzed by several techniques. The presence of small amounts of f-HNT allows good dispersion of the tubes and the subsequent formation of homogeneous gels. The experimental results show that f-HNT functions only as an additive in the hybrid gels and does not demonstrate gelator behavior. The *in vitro* kinetic release from both f-HNT/CPT and Fmoc-F/f-HNT/CPT was studied in media that imitates physiological conditions, and the factors controlling the release process were determined and discussed. Furthermore, the antiproliferative *in vitro* activities of the gels were evaluated towards human cervical cancer HeLa cells. A comparison of data collected in both systems shows the synergistic action of f-HNT and the gel matrix in controlling the release of CPT in the media and maintaining the drug in its active form. Finally, a comparison with pristine HNT is also reported. This study suggests a suitable strategy to obtain two-component gel hybrids based on nanocarriers with controlled drug carrier capacity for biomedical applications.

## Introduction

In recent decades, cancer has become one of the major causes of mortality worldwide; it claims millions of lives each year, and its incidence continues to increase. Despite advances in medicine, chemotherapy has remained the standard treatment for most cancers. Camptothecin (CPT) is a cytotoxic or antineoplastic chemotherapeutic anticancer drug mainly used to treat metastatic colon or rectal cancer. This drug is known as a topoisomerase-I inhibitor. To date, CPT has been used only in injectable form. Unfortunately, CPT is an irritant molecule that can cause vein inflammation and tissue damage. In addition, the major drawback that prevents its oral administration is its low solubility in aqua-based media, along with the low stability of its active form, lactone, which readily hydrolyses into carboxylate at neutral and slightly alkaline pH values.[1]

To overcome the side effects of chemotherapeutic molecules and improve their efficacy, various drug delivery systems have been developed.[2–4] Among these, inorganic nanocarriers such as halloysite are emerging nanomaterials with appealing potential in drug delivery.[5,6]

Halloysite is a natural aluminosilicate clay with a predominantly hollow tubular structure (HNT); it is chemically similar to platy kaolin ($Al_2Si_2O_5(OH)_4$), which shows excellent bio-[7,8] and ecocompatibility.[9,10] Halloysite is positively charged in the inner lumen, which consists mostly of aluminum hydroxide, whereas the external surface, which consists of silicon dioxide,[11] is negatively charged. The different surface chemistry allows selective functionalization of the inner or outer surfaces, enabling the synthesis of nanomaterials with hierarchical nanostructures.[12–14] HNTs are widely used in numerous fields,[15–21] including drug carriers[22–26] and drug delivery.[27] Concerning the use of HNTs as drug delivery systems, maintaining a constant drug concentration is a fundamental issue. However, the relevance of the

[a] Dipartimento STEBICEF, Sez. Chimica, Università degli Studi di Palermo, Viale delle Scienze, Ed. 17, 90128 Palermo, Italy. E-mail: francesca.danna@unipa.it, serena.riela@unipa.it
[b] Dipartimento di Ingegneria Civile, Ambientale, Aerospaziale, dei Materiali, Università degli Studi di Palermo, Viale delle Scienze, Ed. 6, 90128 Palermo, Italy
[c] Institute of Biomedicine and Molecular Immunology, CNR, IBIM, Via Ugo La Malfa, 153, 90146 Palermo, Italy
[d] Dipartimento di Fisica e Chimica, Università degli Studi di Palermo, Viale delle Scienze, Ed. 17, 90128 Palermo, Italy

† Dedicated to Prof. Renato Noto for his brilliant scientific career.

‡ Electronic supplementary information (ESI) available: FT-IR spectra, thermograms, rheological properties and kinetic data. See DOI: 10.1039/c7tb00297a

above problem can be easily reduced by taking advantage of the possibility of incorporating HNTs in semi-solid matrices, such as hydrogels. Hydrogels, due to their hydrophilic character and biocompatibility, have been used for the delivery of drug molecules; most hydrogels are polymeric, with networks consisting of covalently cross-linked natural or synthetic polymers.[28,29] However, the possibility of obtaining hybrid supramolecular hydrogels in the presence of HNTs has not been greatly investigated to date. Compared to polymeric hydrogels, supramolecular hydrogels offer different advantages, such as sol–gel reversibility under the action of different stimuli and the possibility of tailoring their properties to a given application by making small changes in the gelator structure.[30–32]

Among hydrogelators, peptides have received much consideration.[33–35] However, their substantial drawbacks are their high cost and complicated chemical syntheses that require long purification processes. To overcome the abovementioned problems, small molecules such as fluoromethoxycarbonyl amino acids with structural features similar to peptides have been largely used.[36–38] In this context, Fmoc-L-phenylalanine (Fmoc-F) is one of the most widely applied molecules. Fmoc-F can furnish hydrogels with high densities featuring uniform entangled fibers. Recently, Fmoc-F has been used in combination with Fmoc-L-isoleucine to obtain two-component gels with antimicrobial activities.[39]

Bearing in mind the above information, herein, we report a series of supramolecular hybrid gels based on Fmoc-F reinforced with functionalized halloysite nanotubes (f-HNT) (Fig. 1).

In particular, we explored the possibility of obtaining both hydro- and organogels in the presence of pristine HNT (p-HNT) and f-HNT containing covalently linked Fmoc-F on the outer surfaces of the tubes. With the final goal of using the new systems as drug carriers, the effects of CPT loading on the systems were also investigated.

In all cases, the physico-chemical properties of the supramolecular gel–HNT hybrids were studied. Specifically, the thermal stabilities of the gels were investigated using the lead-ball method[40] and micro-DSC (μ-DSC) measurements, whereas their mechanical properties were examined by rheology. Furthermore, the self-repair abilities of the gels were analyzed by subjecting them to ultrasound and magnetic stirring. The morphology of a chosen hybrid hydrogel (discussed later) was investigated by polarizing optical microscopy (POM) and transmission electron microscopy (TEM). The changes in the hydrodynamic radii were investigated in terms of translational diffusion from Dynamic Light Scattering (DLS) measurements. Different behaviors were observed for gel forming (f-HNT in phosphate buffer solution) and non-gel forming (f-HNT in triethylene glycol) systems. The kinetic *in vitro* release of CPT from HNT or the gel matrix was studied in a medium that mimics physiological pH conditions. Finally, the antiproliferative *in vitro* activities of the gels towards human cervical cancer HeLa cells were studied.

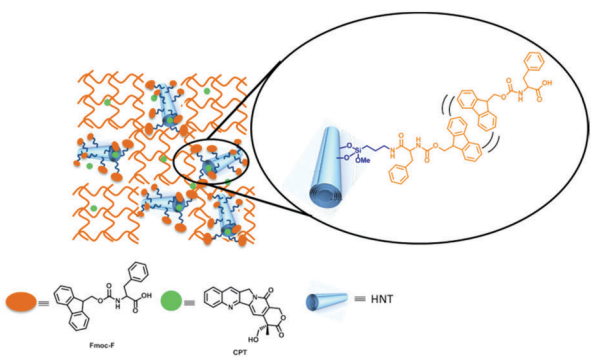


Fig. 1 Representation of the Fmoc-F/f-HNT/CPT hybrid gel.

## Results and discussion

### Synthesis and characterization of filler

**Synthesis of f-HNT.** HNT bearing Fmoc-F units was prepared according to the synthetic route shown in Scheme 1. As previously reported,[41] halloysite nanotubes were reacted with 3-azidopropyltrimethoxysilane in toluene at reflux, affording HNT–$N_3$. After workup, the p-HNT loading of the $N_3$ groups, estimated by TGA, was *ca.* 2.4 ± 0.2 wt%; this nanomaterial represents a versatile starting point for subsequent functionalizations. Quantitative reduction of HNT–$N_3$ with $PPh_3$ afforded amino-functionalized HNT–$NH_2$. The synthesis of f-HNT was carried out by condensation of Fmoc-F to HNT–$NH_2$ in the presence of *N*,*N*′-dicyclohexylcarbodiimide. After workup, we obtained a material with a Fmoc-F loading of 2.3 ± 0.1 wt% with respect to HNT–$NH_2$.

### Loading of camptothecin into f-HNT

The loading of CPT into f-HNT was carried out by mixing halloysite with a highly concentrated aqueous camptothecin solution. Then, the obtained suspension was stirred and maintained under vacuum for 3 to 5 min, resulting in light fizzling, which indicated that air was being removed from the tubes. Once the vacuum was removed, the solution entered the lumen and the loaded compound condensed within the tubes. This procedure was repeated 2 to 3 times to improve the loading efficiency. After loading, the f-HNT/CPT complex was washed with water in order to remove free CPT. CPT-loaded pristine HNT, p-HNT/CPT, was similarly prepared as a reference material. The drug loading of p-HNT/CPT and f-HNT/CPT was estimated by UV-vis spectroscopy. The amounts of CPT loaded in the HNT lumen, expressed as the percent amount of drug in the final composite, were *ca.* 2.1 wt% and 2.7 wt% for p-HNT/CPT and f-HNT/CPT, respectively. TGA loading values confirmed the UV-vis findings, being 1.5 wt% and 2.7 wt% for p-HNT/CPT and f-HNT/CPT, respectively. The different percent loadings of drug in the different carriers may be due to the presence of the Fmoc-F groups on the halloysite surface. This group, indeed, can promote the loading of CPT onto the carriers by means of additional supramolecular interactions, such as π–π interactions, as demonstrated by the different kinetic releases (see below).

The new nanomaterials were characterized by FT-IR spectroscopy and thermogravimetric analysis.

 

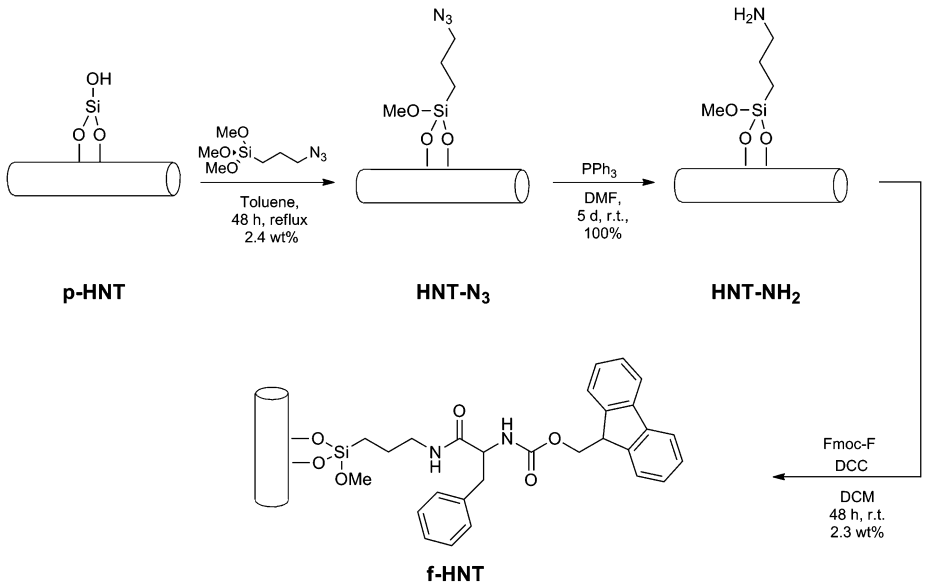


Scheme 1 Synthesis of the f-HNT/CPT hybrid.

### FT-IR spectroscopy

The FT-IR spectra of Fmoc-F, HNT–$NH_2$ and f-HNT are illustrated in Fig. S1a (ESI‡). The bands of the pristine components can be assigned on the basis of literature data for HNT[24] and Fmoc-F.[42] In particular, the FT-IR spectrum of pure Fmoc-F exhibits two C═O stretching peaks at 1736 and 1680 $cm^{-1}$ for the acid and amide carbonyl groups, respectively. The hybrid nanomaterial presents the characteristic bands of both HNT and Fmoc-F, with one major variation: the carbonyl group shifted from 1736 $cm^{-1}$ to *ca.* 1624 $cm^{-1}$. These findings confirm the covalent grafting of Fmoc-F to HNT–$NH_2$ and exclude the presence of adsorbed amino acids on the surface or in the inner lumen of the nanotubes. Fig. S1b (ESI‡) shows the FT-IR spectra of camptothecin and the f-HNT/CPT hybrid. In the pure CPT spectrum, the specific bands of the C═O groups of lactone and pyridone can be found at 1750 and 1650 $cm^{-1}$, respectively. The stretching vibration of aromatic C–C and the bending vibration of C═N both appear at 1579 $cm^{-1}$. The band at ∼1603 $cm^{-1}$ was attributed to aromatic C═C.[43] The FT-IR spectrum of the f-HNT/CPT hybrid system resembled the superimposition of the spectra corresponding to the drug and to the clay, confirming the presence of CPT in the f-HNT.

### Thermogravimetric analyses

Thermogravimetric analyses (TGA) were performed on the obtained nanomaterials; the results confirmed the functionalization on the external surface of HNT and enabled us to calculate the loading of CPT on the f-HNT nanomaterial (2.8 wt%). The curves (Fig. S2, ESI‡) clearly show that the residual of the nanomaterials changed in a stepwise fashion from p-HNT to f-HNT due to the organic compounds linked on the surface of the nanotubes. The thermograms were corrected for the different moisture contents to underline the weight losses of HNT and organic compounds. Above 100 °C, the HNT curve reveals the characteristic weight loss at 500 °C, attributed to the expulsion of two water molecules from the HNT interlayers.[18,44] HNT–$NH_2$ showed an additional weight loss at 250 °C due to the $NH_2$ group.[45] In contrast, f-HNT exhibits a weight loss between 150 °C and 200 °C due to the presence of Fmoc-F (2.3 wt% with respect to HNT–$NH_2$). It is worth noting that camptothecin undergoes a two-step degradation process (Fig. S3, ESI‡). In agreement with the ratio between the weight losses of each degradation step and literature findings, camptothecin presented decarboxylation (282 °C), followed by full degradation (360 °C). The loading of CPT on p-HNT is demonstrated by the weight losses between 200 °C and 400 °C.

Furthermore, the TGA results provided the stoichiometry of f-HNT. Based on the Fmoc-F loading (2.8 wt%), we determined that the mole ratio of Fmoc-F and the amino groups linked on the surface of the HNTs is 1 : 6. It is noteworthy that the f-HNT nanomaterial possesses new Fmoc-F functionalities and some unreacted free amino groups that could cooperate to aid cellular uptake into the cytosol.[46] As expected, the obtained ratio is lower than 1 : 1 due to steric hindrance.

### Morphology of the filler

The morphologies of the pristine and functionalized HNTs were characterized by transmission electron microscopy (TEM). According to the TEM images (Fig. S4, ESI‡), f-HNT shows the typical rod-shaped structure of HNTs, with a diameter of about 100 nm and a length of about 0.7 mm.

### Gelating ability and study of gel properties

Pristine and functionalized halloysite nanotubes were used as fillers for the Fmoc-F hydrogels and organogels. It is worth noting that only biocompatible solvents were used for the gelation tests because the gels are intended for drug release purposes, as discussed above. The results obtained are reported in Table S1 (ESI‡).

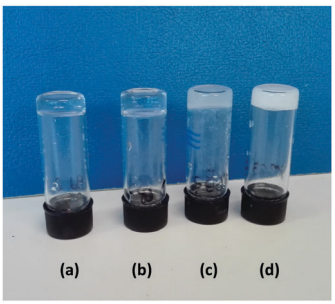


Fig. 2 (a) Transparent hydrogel obtained in PB; (b) transparent hydrogel obtained in PBS; (c) hybrid hydrogel obtained in PBS containing 0.1 wt% f-HNT; (d) white opaque organogel obtained in DEG.

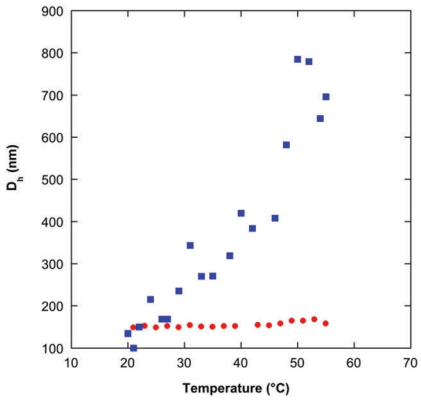


Fig. 3 Hydrodynamic diameters ($D_h$) by dynamic light scattering measurements of Fmoc-F samples with 0.1 wt% in PB (red circles) and 0.5 wt% in triethylene glycol (blue squares).

Among the solvents tested, Fmoc-F was soluble in ethyl-lactate and triethylene glycol, whereas it was insoluble also at low percentages in glycerol, R-limonene and a water/DMSO binary mixture (90 : 10; v : v).

In general, Fmoc-F can be considered to be a super-gelator in water solutions, such as phosphate buffer saline (1×) at pH 7.4 and phosphate buffer solution at pH 7.4 (PBS and PB, respectively); indeed, it was able to gel with critical gelation concentrations (CGC) of 0.1 and 0.2 wt%, respectively, in these buffers.[47] Moreover, in diethylene glycol (DEG), Fmoc-F behaves as a common low molecular weight gelator (LMWG), presenting a CGC of 1 wt% (Table S1, ESI‡). Transparent hydrogels (Fig. 2a and b) stable to the tube inversion test[48] were observed, while a white opaque gel was obtained in DEG (Fig. 2d).

Thus, there is a substantial difference between the hydrogels and organogels in terms of CGC and gel appearance. On the other hand, the thermal stability of Fmoc-F in DEG, measured using the lead-ball method,[40] was slightly lower with respect to Fmoc-F in PB (53.3 °C and 57.7 °C, respectively), despite the significant differences in the CGCs.

A comparison of the data obtained for the hydrogels indicates that the higher ionic strength of PBS solution favours the gelation process with a lower concentration of gelator.

To further analyze the gelation mechanism, the hydrodynamic diameters of aggregates as a function of temperature were assessed by dynamic light scattering (DLS) studies. These experiments were performed under the CGC (on low concentrated solutions) as an ergotic system is required for DLS measurements. To this aim, we chose two representative gelating (Fmoc-F in PB at 0.1 wt%) and non-gelating (Fmoc-F in triethylene glycol at 0.5 wt%) systems. The results, reported in Fig. 3, reveal an interesting phenomenon. Indeed, the Fmoc-F in PB shows no changes in hydrodynamic diameter ($D_h$ = 150 nm) over the entire investigated temperature range, whereas in triethylene glycol, the hydrodynamic diameter changes from 140 to 800 nm (Fig. 3). The obtained results indicate that the formation of the gel network depends on the tendency of the solute to aggregate in the used solvent. In other words, we assume that temperature-induced aggregation, evidenced in the dilute regime, could generate an instable colloidal system that undergoes sedimentation, preventing uniform network formation. This hypothesis perfectly agrees with one previously reported in the literature, which defines the gelation process as an incomplete crystallization.[49]

Once we obtained the supramolecular gels, we analyzed how the introduction of different HNT species influenced their properties. First, we investigated the ability of these species to disturb or contribute to the gelation process by gelation tests (Table 1 and Table S1, ESI‡). Subsequently, properties such as the thermal stability of the hybrid gels were compared to those of pure gels.

The hybrid gels were prepared using a concentration of Fmoc-F equal to those of the CGC values of the pure gels. Opaque homogeneous gels were obtained, as reported in Fig. 2c.

Analysis of the data in Table S1 (ESI‡) underlines that the addition of a small quantity of p-HNT destabilizes the formation of the gel in the case of DEG. On the other hand, in water buffer solutions, the gel formation was not prevented; however, the soft materials obtained were not homogeneous due to the inhomogeneous dispersion of p-HNT in solution.

A different scenario was observed in the presence of f-HNT; indeed, the presence of a small amount of Fmoc-F anchored on the external surface of the HNTs allowed good dispersion of the nanotubes in all solvents used and the subsequent formation of homogeneous gels. The homogeneous dispersion of f-HNT is clearly shown by the TEM images reported in Fig. 4. It should be noted that functionalization of the external surface of the HNTs with the Fmoc-F group is crucial to obtain the "needle-like" structures that allow the formation of homogeneous gels.

In these cases, we were able to compare the $T_{gel}$ values of the pure and hybrid gels (Table 1). In particular, the presence of f-HNT (0.1 wt%) caused a decrease in thermal stability compared to the pure hydrogels (43.8 °C *vs.* 46.3 °C for PBS and 44.9 °C *vs.* 57.7 °C for PB). It is noteworthy that the destabilizing effect was more significant in the case of PB than that of PBS.

Moreover, increasing the f-HNT concentration in the hydrogel matrix further decreased the $T_{gel}$ value of the gel in PBS, whereas it remained almost constant for the gel in PB.

On the other hand, the thermal stability of the organogels does not appear to be influenced by the presence of f-HNT;

 

Table 1 Gelation tests and corresponding $T_{gel}$ values of Fmoc-F in the presence of different species of HNT

| | Solvent | | | | | | | | |
|---|---|---|---|---|---|---|---|---|---|
| | PBS[a] | | | PB[b] | | | DEG[c] | | |
| Filler | Conc.[d] | Appear.[e] | $T_{gel}$[f] | Conc.[d] | Appear.[e] | $T_{gel}$[f] | Conc.[d] | Appear.[e] | $T_{gel}$[f] |
| None | 0 | TG | 46.3 | 0 | TG | 57.7 | 0 | OG | 53.3 |
| p-HNT | 0.1 | NOG | — | 0.1 | NOG | — | 0.1 | I | |
| f-HNT | 0.1 | OG | 43.8 | 0.1 | OG | 44.9 | 0.1 | OG | 54.4 |
| | 0.2 | OG | 31.8 | 0.2 | OG | 43.9 | 0.2 | OG | 51.8 |
| | 0.5 | OG | 32.6 | 0.5 | OG | 41.4 | 0.5 | I | |
| p-HNT/CPT | 0.1 | OG | 44.1 | 0.1 | OG | 45.9 | 0.1 | I | |
| f-HNT/CPT | 0.1 | OG | 42.1 | 0.1 | OG | 51.4 | 0.1 | I | |

[a] Fmoc-F at 0.1 wt%. [b] Fmoc-F at 0.2 wt%. [c] Fmoc-F at 1 wt%. [d] Concentration of material in the gel, (%, w/w). [e] Appearances: TG = transparent gel; OG = opaque gel; NOG = non-homogeneous gel; I = insoluble. [f] (°C), $T_{gel}$ determined by the lead ball-method and reproducible within 1 °C.

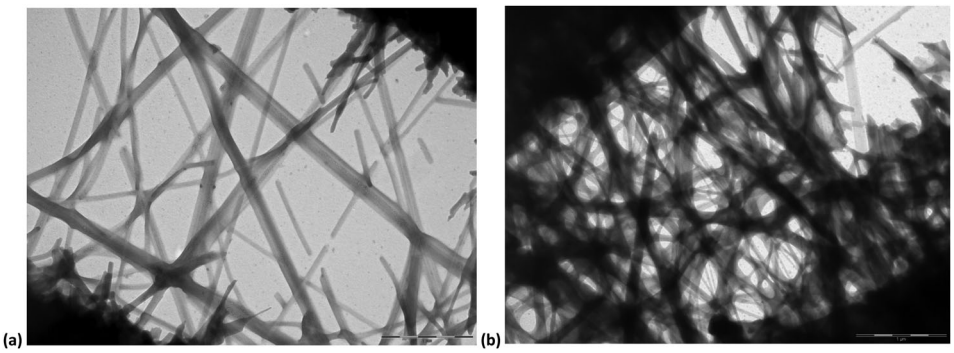


Fig. 4 TEM images of the hybrid gels in PBS: (a) at 0.3 wt% Fmoc-F and (b) 0.1 wt% f-HNT.

however, a concentration higher than 0.2 wt% was found to prevent organogel formation.

In addition, in the case of the hydrogels, we tested the ability of f-HNT to induce gelation for mixtures with concentrations of Fmoc-F lower than the CGC (Table S1, ESI‡); however, we were unsuccessful. Thus, we can assert that f-HNT functions only as an additive as it cannot behave as a gelator; however, the addition of f-HNT to the gel network affects the properties of the soft materials obtained.[50] In light of the abovementioned results, we analyzed the effects of the presence of p-HNT/CPT and f-HNT/CPT. In these cases, we decided to use the smallest amount of material corresponding to 0.1 wt% as, from previous results, it appears that nanotubes can negatively influence the thermal stabilities of gels.

Surprisingly, we obtained homogeneous hydrogels with both materials; probably, the small loading of an additional organic molecule on p-HNT allows homogeneous dispersion of the nanotubes in solution and the subsequent formation of gels. Incidentally, both CPT-materials prevented the formation of organogels, further indicating the completely different behaviours of the hydrogels and organogels. The thermal stabilities of the hybrid gels loaded with CPT follow the trend explained above for the f-HNT gels. Indeed, decreases in the $T_{gel}$ values were observed with respect to those of the pure gels. However, no significant variations were determined with respect to the hybrid gels. With the aim of using the hydrogels as drug delivery systems, tests were performed using concentrations of 0.3 wt% Fmoc-F and 0.1 wt% f-HNT or f-HNT/CPT. Indeed, a concentration higher than CGC should result in a gel with higher strength and thermal stability. These properties may be necessary to resist contact with the release phase at 37 °C.

In particular, for the abovementioned samples, their thermal stabilities, as assessed by both μ-DSC and the lead-ball method as well as their, rheological behaviours, morphologies and self-recovery abilities were investigated.

## Thermal properties

μ-DSC experiments were carried out by heating the gel samples. The baseline was subtracted as previously reported.[51] A representative thermogram is shown in Fig. S5 (ESI‡). The asymmetric shape evidences a first order transition, typical of temperature-induced self-aggregating systems.[52] This implies that the molecules form aggregates that break down the gel network at high temperatures. This mechanism was also highlighted by the DLS results.

Table 2 shows that the temperatures at which the gel-to-liquid phase transition occurs are around 75 °C for Fmoc-F in PBS and 65 °C in PB. This difference is due to the different saline content of PBS compared to PB; this is also confirmed by the values determined with the lead-ball method.

The $T_{gel}$ values obtained in the latter case were lower than those observed using μ-DSC. According to a previous report,[53] this may be due to differences in the observed phenomena, *i.e.* in the first case, the loss of strength in the gel network and the complete clarification in the second case.

The $T_{gel}$ appears to decrease slightly upon addition of HNTs, according to the previously discussed trend for thermal stability

Table 2 Melting enthalpy of gel phases ($\Delta H_{gel}$), onset and gelation temperature of melting ($T_{gel}$) for the pure hydrogels (Fmoc-F in PB and PBS) and the hybrid hydrogels (Fmoc-F/f-HNT in PBS or PB and Fmoc-F/f-HNT/CPT in PB or PBS) at concentrations of 0.3 wt% Fmoc-F and 0.1 wt% f-HNT. The numbers in brackets are the $T_{gel}$ values determined with the lead-ball method

| | PBS | | | PB | | |
|---|---|---|---|---|---|---|
| Material | $\Delta H_{gel}$ [J g$^{-1}$] | Onset [°C] | $T_{gel}$ [°C] | $\Delta H_{gel}$ [J g$^{-1}$] | Onset [°C] | $T_{gel}$ [°C] |
| None | 32 | 77.9 | 78.8 (60.0) | 25 | 66.9 | 67.4 (54.9) |
| f-HNT | 34 | 74.2 | 75.3 (66.5) | 23 | 64.7 | 65.4 (53.7) |
| f-HNT/CPT | 34 | 74.0 | 75.0 (62.3) | 23 | 64.2 | 65.0 (53.4) |

at CGC values. In contrast, the enthalpy of melting $\Delta H_{gel}$ [J g$^{-1}$] was not influenced by the filler. CPT influences neither the enthalpy nor the temperature.

### Rheological properties

The rheological properties of the pure and hybrid gels were investigated at room temperature. It is worth mentioning that in this case, we also analyzed the behaviour of the organogels at concentrations of 1.5 wt% Fmoc-F and 0.1 wt% f-HNT.

Variations of the elastic modulus, $G'$, and the viscous modulus, $G''$, as a function of the percentage of strain ($\gamma$) and angular frequency ($\omega$) were examined within the linear viscoelastic region (LVR) of the gels.

All the analyzed samples behaved as gel phases, presenting the classic intermediate behaviour between solids and liquids.[54,55] Indeed, in strain sweep measurements at low values of $\gamma$, a solid-like behaviour with $G'$ higher than $G''$ was detected. However, the further increase of $\gamma$ reached a crossover point after which $G' < G''$, indicating liquid-like behaviour.

Furthermore, it was possible to measure the gel strength from the crossover points of yield strain ($\gamma$ at which $G' = G''$) and the loss tangents ($\tan\delta = G''/G'$). Usually, the stronger the gel, the higher the crossover point of $\gamma$ and the lower the $\tan\delta$ value (Table 3).

The rheological properties greatly varied depending on the solvent used and in the presence of different halloysite nanotubes (Fig. 5 and Fig. S6, ESI‡).

A comparison of the data obtained for the hydrogels and organogels, once again, indicates the different behaviours induced by the nature of the solvent. Indeed, even when the $\tan\delta$ values are comparable, the organogels present $G'$ values two orders of magnitude higher than those of the hydrogels. Furthermore, an unusual dependence of the loss modulus on the angular frequency can be observed; specifically, a concave trend of $G''$ in respect to $G'$, instead of the classical parallel evolution of the two moduli, is observed (Fig. 5b). This behaviour is usually reported for strong polymeric gels.[56,57] However, interestingly, the organogels flow at a lower value of strain than the hydrogels. The presence of f-HNT and f-HNT/CPT does not significantly influence the mechanical properties of the hydrogels in terms of the moduli and $\tan\delta$ values (Fig. 5c and d); however, an interesting variation in the crossover point is observed for pure hydrogels compared to hybrid hydrogels. In general, the addition of HNT nanomaterials increases the percentage of strain needed to flow the gel, generating a stronger soft material. However, the presence of CPT anchored in f-HNT probably induced different interactions between the nanotubes and the gelator. For example, in PBS gel, the elastic modulus is comparable with that of the pure gel but higher than that of Fmoc-F/f-HNT in PBS, while the opposite trend is observed for the crossover point.

On the other hand, in the case of PB gel, further functionalization of the material causes a decrease in the elastic modulus but a concomitant increase in the crossover point. Therefore, it is possible to assert that the functionalization of the material strongly affects not only the gel formation but also its intrinsic properties.

In general, functionalized halloysite nanotubes appear to be beneficial elements for hydrogel stability. In contrast, the presence of f-HNT destabilizes the mechanical response of the organogels, with a decrease of all studied parameters.

### Thixotropic and sonotropic behaviour

An important property of gels is their ability to self-repair after disruption caused by external stimuli, such as magnetic stirring (thixotropy) and ultrasound irradiation (sonotropy). Considering the pharmaceutical application of these gels as drug delivery systems, we were also interested to test these properties.[58,59] The results obtained after submission of the gels to these external stimuli are reported in Table 4 in terms of the thixotropic or sonotropic behaviour of the gels.

In general, the hybrid gels retained the properties of the pure gels; the only exception was Fmoc-F/f-HNT in PBS, which was stable after ultrasound irradiation. All the hydrogels gave good responses to the thixotropic tests, demonstrating self-repair

Table 3 $G'$, $G''$ and $\tan\delta$ at $^a\gamma$ = 1%, $^b\gamma$ = 0.025% and $\gamma$ at $G' = G''$ for the gels at gelator concentrations of $^a$0.3 wt%, $^b$1.5 wt% and 0.1 wt% HNT at 25 °C. Error limits are based on the average of three different measurements with different aliquots of gel

| Gel | $G'$ (Pa) | $G''$ (Pa) | $\tan\delta$ | $\gamma$ at $G' = G''$ (%) |
|---|---|---|---|---|
| Fmoc-F in PBS | $740 \pm 15^a$ | $100 \pm 8^a$ | $0.14 \pm 0.01^a$ | $150 \pm 10$ |
| Fmoc-F/f-HNT in PBS | $590 \pm 70^a$ | $76 \pm 6^a$ | $0.130 \pm 0.007^a$ | $250.3 \pm 0.1$ |
| Fmoc-F/f-HNT/CPT in PBS | $780 \pm 40^a$ | $110 \pm 7^a$ | $0.14 \pm 0.01^a$ | $110 \pm 50$ |
| Fmoc-F in PB | $440 \pm 20^a$ | $40 \pm 4^a$ | $0.09 \pm 0.03^a$ | $160 \pm 90$ |
| Fmoc-F/f-HNT in PB | $530 \pm 60^a$ | $60 \pm 10^a$ | $0.108 \pm 0.008^a$ | $250 \pm 1$ |
| Fmoc-F/f-HNT/CPT in PB | $240 \pm 15^a$ | $25 \pm 3^a$ | $0.10 \pm 0.02^a$ | $406 \pm 10$ |
| Fmoc-F in DEG | $28000 \pm 8500^b$ | $4100 \pm 1800^b$ | $0.14 \pm 0.03^b$ | $20 \pm 5$ |
| Fmoc-F/f-HNT in DEG | $11800 \pm 300^b$ | $2100 \pm 30^b$ | $0.178 \pm 0.007^b$ | $15.8 \pm 0.1$ |

 

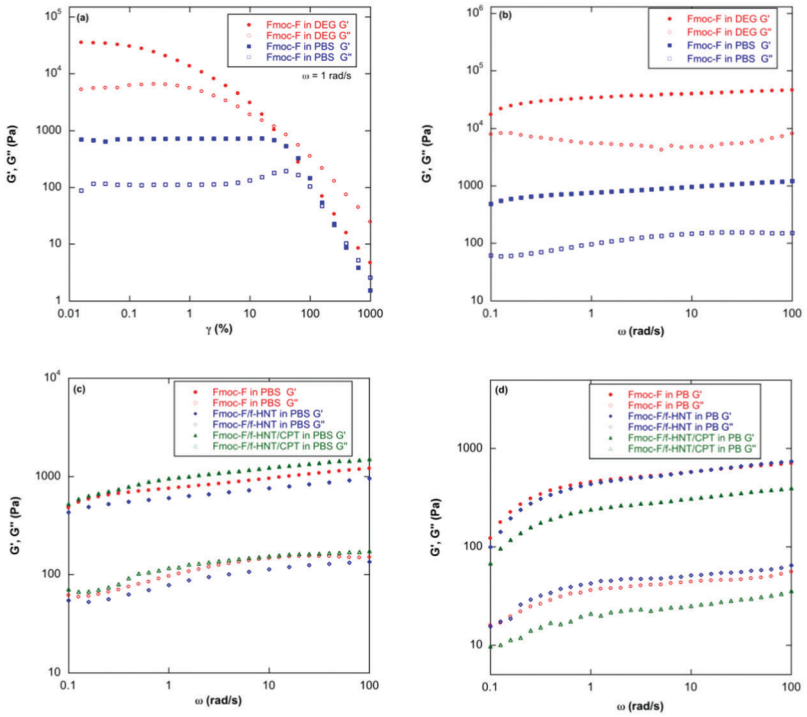


Fig. 5 (a) Strain sweeps of organogels and hydrogels; (b) frequency sweeps of organogels and hydrogels at $\gamma$ = 0.025% and 1%, respectively; (c) frequency sweeps of pure and hybrid hydrogels formed in PBS at $\gamma$ = 1%; (d) frequency sweeps of pure and hybrid hydrogels formed in PB at $\gamma$ = 1%.

Table 4 Self-healing abilities at 0.3 wt% or 1.5 wt% Fmoc-F of the hydrogels and organogels, respectively; all hybrid gels contained 0.1 wt% f-HNT

| Gel | Sonotropy | Thixotropy |
|---|---|---|
| Fmoc-F in PBS | Yes | Yes |
| Fmoc-F/f-HNT in PBS | Stable | Yes |
| Fmoc-F in PB | Stable | Yes |
| Fmoc-F/f-HNT in PB | Stable | Yes |
| Fmoc-F in DEG | No | No |
| Fmoc-F/f-HNT in DEG | No | No |

after disruption, while most of the hydrogels were stable to ultrasound irradiation. The behaviour of the organogels was once again totally opposite to that of the hydrogels as they showed neither sonotropic nor thixotropic properties.

The self-repairing abilities of the hydrogels were further confirmed by rheological analysis. In particular, the pure hydrogels in PBS after exposure to ultrasound irradiation presented classical gel phase behaviour, as shown by the frequency and strain sweep results (Fig. S7, ESI‡). These data clearly indicate the complete recovery of the moduli after gel disruption, although a partial loss of the gel strength was observed from the crossover point that existed at 50% of strain instead of 150%. On the other hand, Fig. 6 and Fig. S8 (ESI‡) show the self-repairing abilities of the gel phases after mechanical disruption. Indeed, when low levels of strain were applied after the disruption of the gels, $G'$ was higher than $G''$, demonstrating their recovery. Furthermore, all the gels completely recovered their initial storage moduli; indeed, the $G'$ values recorded in the linear

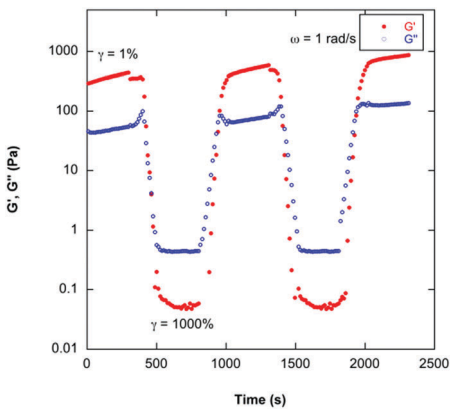


Fig. 6 $G'$ and $G''$ as a function of time at low ($G' > G''$ regimes, $\gamma$ = 1%) and destructive strain ($G'' > G'$ regimes, $\gamma$ = 1000%) for the hybrid hydrogel with f-HNT in PB.

viscoelastic region after disruption were equal to the initial values (≈100% of $G'$ recovery). This behaviour indicates the power of the gelator to rapidly reorganize, forming a gel network with the initial strength; Weiss *et al.* recently reported a similar trend, where they obtained a recovery of 90% for $G'$ after the reformation of a supramolecular gel subsequent to mechanical disruption.[60]

## Morphology of the gel phases

The hydrogel phases were further characterized by POM and TEM measurements (Fig. 7). In particular, we chose to analyze the morphologies of both the pure and CPT-hybrid gels in PBS.

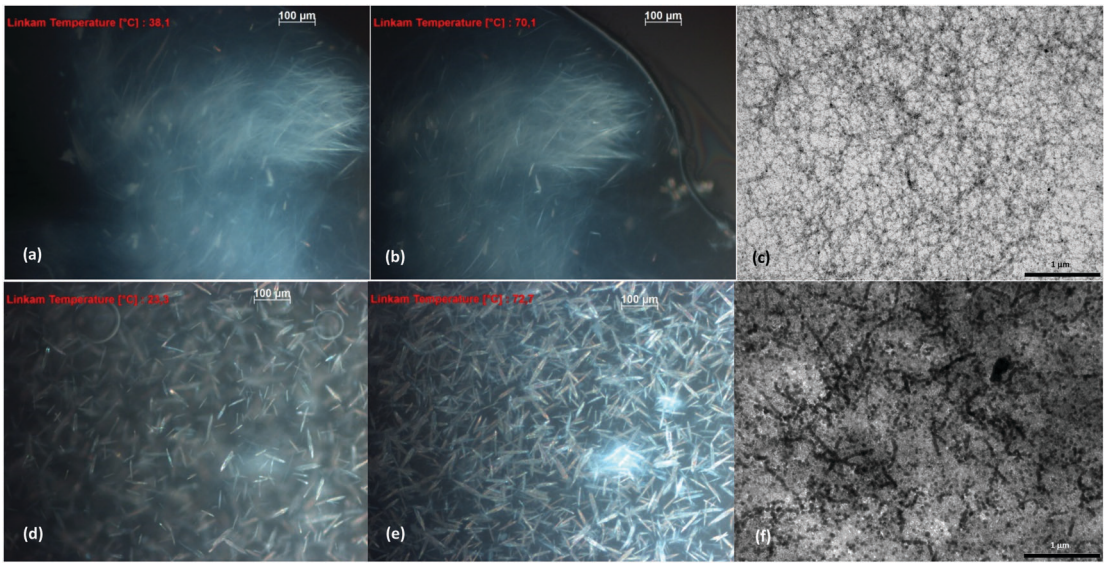


Fig. 7 Morphological images of the pure and CPT-hybrid gels in PBS at 0.3 wt% Fmoc-F and 0.1 wt% f-HNT/CPT: (a) POM image of the pure gel at 38.1 °C; (b) POM image of the pure gel at 70.1 °C; (c) TEM image of the pure gel at room temperature; (d) POM image of the CPT-hybrid gel at room temperature; (e) POM image of the CPT-hybrid gel at 72.7 °C; (f) TEM image of the CPT-hybrid gel at room temperature.

Indeed, the latter showed the best performance in the CPT release process (discussed later) and was stronger than the CPT-hybrid gel obtained in PB (Table 3).

First, the images obtained of the pure gel (Fig. 7a–c) clearly indicate the presence of a fibrous structure. According to previous reports in the literature, the fibres are quite entangled and they also persist at temperatures higher than the $T_{gel}$ value (43.8 °C; Fig. 7b). This observation recalls the DLS data in PB, which show that the aggregate diameters remain unchanged despite the temperature increase. According to the initial analysis by POM measurements, the incorporation of f-HNT/CPT in the gel matrix seems to induce a change in the morphology. Indeed, at 23.3 °C, in a dense gelatinous matrix, we observed the presence of a "needle-like" reticular structure (Fig. 7d); moreover, in this case, the lattice persists at temperatures higher than the $T_{gel}$ value (42.1 °C; Fig. 7e).

However, according to the TEM measurements from a deeper inside of gel matrix, it can be seen that the dense fibrous network observed in the pure gel persists in the presence of f-HNT/CPT (Fig. 7f and Fig. S9, ESI‡). In addition, the nanotubes are homogeneously dispersed on the gel matrix and are clearly recognizable as they are darker than the gel fibers.

### Kinetic release

The kinetic release of the drug from all studied systems was analyzed at pH 7.4 and at 37 °C in order to mimic typical physiological conditions. This study was carried out for both the hybrid HNT and gel matrices.

### CPT release from the HNT hybrids

The controlled release of CPT from both HNT hybrids was studied in PB at pH 7.4. Regarding the CPT release from the p-HNT/CPT system, an anomalous increase in the absorbance intensity and a slight blue shift of the maximum absorbance were observed; this complicated the data analysis. This phenomenon is due to the formation of CPT aggregates by stacking interactions in the release medium; this explains the increasing height of the corresponding peaks in the experimental spectra.[61] The CPT release-time profiles from p-HNT/CPT and f-HNT/CPT are reported in Fig. S10 (ESI‡). Both systems exhibited sustained release of CPT with an initial rapid-release phase, followed by a gradually slower release pattern. The cumulative releases of CPT were around 69% and 34% for p-HNT and f-HNT, respectively, after 12 h and 100% in both cases after 120 h. These results suggest that both HNT hybrids are capable of sustaining the release of CPT over at least 4 days.

In order to study the release mechanism, the release data were analyzed according to the power fit equation and an equation in the form:

$$F_t = M_\infty \cdot (1 - e^{-k_1 t}) + k_0 t \quad (1)$$

*i.e.* providing the sum of an exponential and a linear term, where $k$ is the kinetic release constant and $n$ is the characteristic diffusion exponent, depending on the release mechanism.

It was found that the release of CPT from the p-HNT/CPT hybrid was controlled by a drug diffusion process ($n = 0.185 \pm 0.005$); moreover, the kinetic data of the release of CPT from f-HNT can be analyzed with both double-term release kinetic and power fit models (Table 5).

The two different behaviors can be explained by the presence of Fmoc-F grafted on the external surface of the HNTs. Indeed, the CPT molecules are released from the HNT inner lumen by a diffusion process; supramolecular interactions (π–π) can then occur with the amino acidic portion. Therefore, we observed the superimposition of two distinct processes, namely a first-order process and a relatively faster zero-order process; *i.e.* the diffusion of drug molecules from the HNT inner lumen and the subsequent release from the external surface.

 

Table 5 Kinetic parameters for CPT release from both HNT hybrids

| | Power fit | | | Double-term | | |
|---|---|---|---|---|---|---|
| | $k$ ($h^{-1}$) | $n$ | $R^2$ | $k_1$ ($h^{-1}$) | $k_0$ ($h^{-1}$) | $R^2$ |
| p-HNT | 43.9 ± 0.6 | 0.185 ± 0.005 | 0.993 | 4.9 ± 1.3 | 0.61 ± 0.08 | 0.925 |
| f-HNT | 10.6 ± 1.8 | 0.48 ± 0.03 | 0.984 | 0.46 ± 0.08 | 0.95 ± 0.03 | 0.996 |

To support these hypotheses, it is noteworthy that the CPT released from the f-HNT hybrid (stoichiometric ratio between amino acid and CPT of 1 : 1) did not form aggregates in aqueous medium as a consequence of its strong interaction with Fmoc-F. It is noteworthy that the loading of CPT into the HNT lumen prevents hydrolysis of the lactone ring, as verified by UV-vis spectroscopy. Indeed, the UV-vis spectrum of CPT released from the HNT lumen after 96 h resembled the UV-vis spectrum of free CPT (Fig. S11, ESI‡).[1]

### CPT release from the Fmoc-F/HNT hybrid gels

The release of CPT from the hybrid gels was also studied to verify if incorporation of HNTs into the gel matrix could induce a time-controlled drug release process. To pursue this goal, we analysed the kinetics of release first from a gel in the presence of CPT alone and subsequently from the hybrid gels.

Pictures of the experimental system used and the calibration curves of CPT in both water buffers are reported in Fig. S12 and S13 (ESI‡).

The trends of cumulative CPT release from both the pure and hybrid gels as a function of time are displayed in Fig. 8, while the relative intervals of time are shown in Tables S2–S4 (ESI‡).

The release of CPT from the pure gel shows an induction period (~2.5 h), after which a linear trend results. The observed trend may be due to normal diffusion, first across the gel and subsequently through the gel (Fig. 8, green plot). However, the low solubility of CPT in the hot suspension used to prepare the soft material gave rise to an inhomogeneous distribution of the drug in the gel matrix, raising issues of reproducibility.

In contrast, in the case of the hybrid gel formed in the presence of f-HNT, we observed a gradual slow release pattern. In particular, according to eqn (4),[62] the $n$ values reported in Table 6 ($n$ = 0.96 ± 0.04 and 0.76 ± 0.04 for Fmoc-F/f-HNT/CPT in PB and for Fmoc-F/f-HNT/CPT in PBS, respectively) refer to a non-Fickian mode of transport, where morphological changes are abrupt and demonstrate the relevance of the gelation solvent.

Table 6 Release constants for hybrid gels containing CPT

| Release medium | Gel | $k$ ($h^{-1}$) | $n$ | $R^2$ |
|---|---|---|---|---|
| PBS | Fmoc-F/f-HNT/CPT in PBS | 0.062 ± 0.002 | 0.70 ± 0.04 | 0.955 |
| PB | Fmoc-F/f-HNT/CPT in PB | 0.126 ± 0.004 | 0.96 ± 0.04 | 0.976 |

According to the $k$ values, the hybrid gel in PBS appears to be the best system for drug release purposes; it is the most resistant and presents a slower release, which is preferable for CPT use in pharmaceutical applications.

A comparison of the data collected for the release from HNT hybrids clearly evidences the synergistic action of the HNTs and the gel matrix; this is shown by the best drug dispersion due to the presence of the filler and the slower rate of release as a consequence of the incorporation of HNTs in the gel phase.

On the basis of the obtained results, the halloysite hybrid supramolecular hydrogel can be used as a good alternative to delivery of CPT in the body by oral dosage, with prolonged therapeutic effects with respect to the traditional injectable form.

### *In vitro* cytotoxicity assay

In order to validate the efficiency of the obtained Fmoc-F/f-HNT/CPT hybrid gels, some preliminary *in vitro* cytotoxicity studies were performed. In particular, we tested the effects of Fmoc-F/f-HNT/CPT hybrid gel in PBS on human cervical cancer HeLa cells by means of the MTS assay (Fig. 9). The survival rates of the tumor cells incubated with Fmoc-F/f-HNT in PBS for 24 h at each concentration were found to be in the range of 96% to 100%,

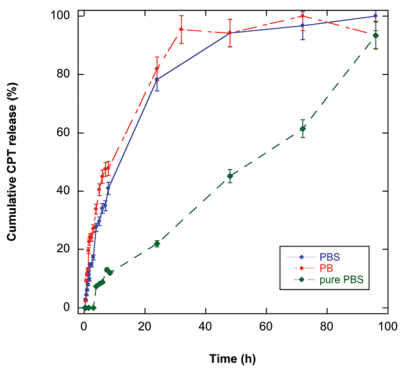


Fig. 8 Percentage of cumulative CPT release at 37 °C as a function of time from the pure Fmoc-F hydrogel in PB + 0.1 wt% CPT (green plot) and from the hybrid Fmoc-F/f-HNT/CPT hydrogel in PBS (blue plot) and PB (red plot).

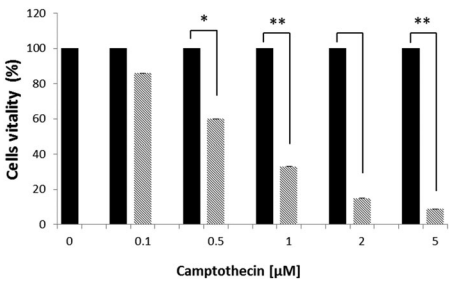


Fig. 9 Anti-proliferative effects of CPT on HeLa cells. Growth inhibition of HeLa cells exposed to camptothecin at different concentrations, from 1 × $10^{-7}$ M to 5 × $10^{-6}$ M at 24 h, measured by MTS assay. Data are mean ± SD from two independent experiments performed in triplicate. The results were compared with values from cells incubated in the absence of CPT (control). *$p < 0.05$ and **$p < 0.01$ were considered to be statistically significant.

indicating that the hybrid gel has no effect on the cell viability of the tumor cell lines under the concentration conditions investigated. In contrast, the cell line showed a dose-dependent cytotoxic profile when subjected to treatment with the Fmoc-F/f-HNT/CPT hybrid gel.

## Conclusions

In summary, new innovative hybrid supramolecular gels have been fabricated for drug release processes. In particular, the hybrid hydrogels reveal efficient, controlled sustained release of CPT, a topoisomerase-I inhibitor drug exhibiting high antitumor activity.

Deep investigation of the hybrid gel properties and comparison with those of the pure gels show that the HNTs behave as an additive in gel network formation; they induce a decrease in thermal stability but, in general, induce a concomitant increase in gel strength.

As demonstrated by TEM images, the f-HNTs are homogeneously dispersed in the gel matrix; thus, the entangled fibrous gel structure is maintained in the hybrid gels. The fabrication of hybrid supramolecular gels such as those that can be obtained in the presence of HNTs has been proved to enable modulation of the properties of hydrogels; the wide range of these gels can offer a plethora of different applications.

In particular, in our case, only the combined action of HNTs and gel produces a delivery system that enables control of the concentration of CPT in the release phase over time. Indeed, f-HNT addresses the issue of drug solubility both in buffer solution and the gel matrix, on the other hand the inclusion of f-HNTs further slows the rate of release. Furthermore, preliminary *in vitro* cytotoxicity assays showed that CPT delivered by the hybrid gels exerts remarkable antiproliferative activities *versus* human cervical cancer HeLa cells.

In addition, over the entire release time, the hybrid materials analyzed in this paper could retain CPT in its lactone active form; this could help overcome issues of drug stability.

Although supramolecular gels have been previously used for drug delivery, very few papers have analysed the possibility of using hybrid supramolecular gels formed in the presence of HNT. To the best of our knowledge, supramolecular hybrid gels are commonly obtained with carbon nanotubes, which are expensive and potentially toxic; in contrast, HNTs are naturally available, inexpensive, and biocompatible. In addition, the hybrid gels prepared in this paper have the dual advantage of allowing sustained release of CPT and preventing its hydrolysis, which represents a drawback of its formulation.

In conclusion, we expect that the obtained materials could be used as a good alternative to drug delivery by oral administration, with suitable prolonged therapeutic effects.

## Experimental section

Fmoc-F and CPT were commercially available (Sigma Aldrich). The solvents were of the highest commercially available grade and were used as received. All reagents needed for the functionalization (Sigma) were used without further purification.

Halloysite was purchased from Sigma-Aldrich. This material has an average tube diameter of 50 nm and an inner lumen diameter of 15 nm. The typical specific surface area of this halloysite is 65 $m^2\ g^{-1}$, with a pore volume of $\sim$1.25 $cm^3\ g^{-1}$, a refractive index of 1.54 and a specific gravity of 2.53 g $cm^{-3}$.

FT-IR spectra in KBr were determined at room temperature in the spectral region of 400 to 4000 $cm^{-1}$ by means of an FT-IR spectrophotometer (Agilent Technologies Cary 630). An average of 30 scans per sample using a nominal resolution of 4 $cm^{-1}$ was registered.

UV-vis measurements were performed using a Beckmann DU 650 spectrometer.

HNT–$N_3$ and HNT–$NH_2$ were prepared as previously reported.[25]

### Synthesis of f-HNT

Fmoc-F (300 mg, 10 eq.) was suspended in $CH_2Cl_2$ (10 mL), and *N*,*N*-dicyclohexylcarbodiimide (160 mg, 10 eq.) was added. The suspension was stirred under an argon atmosphere at room temperature for 10 min. Then, HNT–$NH_2$ (500 mg) was quickly added. The mixture was stirred for 48 h. Then, the solvent was removed by filtration; the powder was then rinsed successively with $H_2O$ and $CH_2Cl_2$ and finally dried at 80 °C under vacuum.

### Loading of camptothecin on the HNT nanomaterials

To a dispersion of p-HNT or f-HNT in deionized water (5 mL), 1 mL of $10^{-2}$ M camptothecin in $CHCl_3$/MeOH (4 : 1) was added. The suspension was sonicated for 5 min at an ultrasound power of 200 W and at 25 °C. The obtained dispersion was stirred for 24 h at room temperature. After this time, the powder was washed with water and then dried at 60 °C under vacuum. The loading efficiency was calculated according to the original concentration of camptothecin and the concentration of unloaded molecules, quantified by means of UV-vis spectrophotometry at a monitoring wavelength of 366 nm. The loading percentage of CPT into the HNT lumen was also calculated by dividing the mass of the encapsulated molecules by the mass of the molecules loaded into the HNT nanomaterials.

### Preparation of gels and $T_{gel}$ determination

The pure gels were prepared by weighing the amount of Fmoc-F and solvent ($\sim$500 mg) into a screw-capped sample vial (diameter 1.5 cm). The mixture was first dispersed for 5 minutes with ultrasound irradiation and subsequently heated in an oil bath at 80 °C until a clear solution was obtained. The vial was then cooled and stored at room temperature overnight. The hybrid gels were prepared by weighing the amounts of Fmoc-F, halloysite materials and solvent ($\sim$500 mg) into a screw-capped sample vial (diameter 1.5 cm). The mixture was first dispersed for 30 minutes with ultrasound irradiation and subsequently heated in an oil bath at 80 °C until a homogeneous dispersion of the hybrid system was obtained. In order to retain a homogeneous dispersion of halloysite in the hot solution, the system was irradiated again in the ultrasonic bath before cooling and storing at room temperature overnight. The tube inversion test method was used to examine the gel formation.[63]

 

To determine the $T_{gel}$ values, a lead ball (weighing 46.23 mg and 2 mm in diameter) was placed on top of the gel, and the vial was placed in a water bath. The bath temperature was gradually increased (2 °C $min^{-1}$) until the gel melted and the lead ball reached the bottom of the vial ($T_{gel}$). The $T_{gel}$ values were reproducible within 1 °C.

### Rheological measurements

The rheology measurements were recorded at room temperature on an ARES G2 (TA Instruments) strain-controlled rheometer using a plate–plate (PP 25-2) tool; the sample was placed between the shearing plates of the rheometer. The rheological properties, such as strain sweep and frequency sweep, were recorded three times on three different aliquots of gels. The strain sweeps were performed at an angular frequency of 1 rad $s^{-1}$ and the frequency sweeps were performed at strains of 1% and 0.025% for the hydrogels and organogels, respectively. These values were chosen to be within the linear viscoelastic region (LVR) of the gels.

The self-repairing properties of the gel phases were also tested using the rheometer; these tests were carried out at room temperature and at an angular frequency of 1 rad $s^{-1}$, varying the strain from low to high percentage values for fixed time intervals of 5 minutes (the values of yield strain to apply were chosen from the linear viscoelastic region and destructive strain of each gel). The rotational strain was maintained at 0% for 0.05 s before changing from destructive strain to linear viscoelastic region conditions. When the moduli reached plateau values after the cessation of disruptive strain, the percentage of recovery of the initial $G'$ value could be calculated.

### Thixotropic and sonotropic behaviour

The obtained gel phases were subjected to two different external stimuli. The mechanical stimulus involved stirring the gel phase with a stirring bar 8 mm in length and 3 mm in height at 1000 rpm for 5 min. The sonotropic behaviour of the gel phases was tested by irradiation in an ultrasound water bath for 5 min with a power of 200 W and a frequency of 45 kHz. Then, the materials were stored at room temperature overnight.

When the samples were stable to the tube-inversion test, the gels were defined as thixotropic or sonotropic.

### Thermogravimetry

The experiments were performed using a Q5000 IR apparatus (TA Instruments) under a nitrogen flow of 25 $cm^3$ $min^{-1}$ for the sample and 10 $cm^3$ $min^{-1}$ for the balance. The mass of each sample was *ca.* 5 mg. The calibration was carried out by means of the Curie temperatures of standards (nickel, cobalt, and their alloys). The sample was heated from room temperature to 900 °C with a scanning rate of 20 °C $min^{-1}$. The degradation temperature ($T_d$) was acquired at the maximum of the first order derivative curve of mass loss *versus* temperature (DTG curves).

### μ-DSC measurements

The gel–sol transitions were recorded on a micro-DSC III (SETARAM) under nitrogen flow in the range from 0 °C to 90 °C with a scan rate of 0.8 °C $min^{-1}$. The stainless steel (1 $cm^3$) sample cell was filled with *ca.* 500 mg of hydrogel, and the reference cell was filled with the corresponding amount of solvent. The calibration was performed using naphthalene.

### Dynamic light scattering (DLS)

Dynamic light scattering experiments were carried out using a Zetasizer NANO-ZS (Malvern Instruments). The field-time autocorrelation functions are well described by a single decay, which provides the decay rate ($\Gamma$) of the diffusive mode. For the translational motion, the collective diffusion coefficient ($D$) at a given concentration is $D = \Gamma/q^2$, where $q$ is the scattering vector given by $4\pi n\lambda^{-1}\sin(\theta/2)$; $n$ is the water refractive index, $\lambda$ is the wavelength (632.8 nm) and $\theta$ is the scattering angle (173°). The field-time autocorrelation functions were also analysed by inverse Laplace transformation, providing the distributions of the hydrodynamic diameters.

### TEM measurements

For TEM observations, the samples were prepared by placing a drop of suspension solution on a formvar-coated copper grid (400 mesh) and allowing the drop to dry completely in a vacuum desiccator. The TEM images of the samples were obtained using a Philips TEM CM 100 transmission electron microscope at accelerating voltage = 80 kV.

### POM measurements

The samples were casted between two glasses to record the POM images. The samples were heated to their sol phases and cooled. The instrument used was a Zeiss Imager.A2m microscope equipped with crossed polarizers, a Zeiss AX10 heating stage, a Photometrics AXIOCAM ICC1 camera interfaced to a computer, and a Linkam microprocessor thermometer connected to a K thermocouple.

### Kinetic release

The release of CPT from the f-HNT/CPT hybrid was determined as follows: 10 mg of the sample were dispersed in 1 mL of phosphate buffer (pH 7.4) and transferred to a dialysis membrane (Medicell International Ltd MWCO 12-14000 with a diameter of 21.5 mm). The membrane was then placed in a round-bottom flask containing 9 mL of the release medium at 37 °C and stirred.

At fixed times, 1 mL of the release medium was withdrawn and analyzed. To maintain the volume of the release medium, 1 mL of fresh solution was added each time to replace the withdrawn volume.

The CPT concentration in the solution was determined by UV-vis spectrophotometry using the Lambert–Beer law. To determine the actual CPT concentration released, the calibration curve was calculated after storage of the standard solution for 24 h at 37 °C.

The total amounts of drug released ($F_t$) were calculated as follows:

$$F_t = V_m C_t + \sum_{i=0}^{t-1} V_a C_i \quad (2)$$

where $V_m$ and $C_t$ are the volume and concentration of the drug at time $t$, respectively. $V_a$ is the volume of the withdrawn sample, and $C_i$ is the drug concentration at time $i$ ($i < t$).

To determine the release mechanism, the amount of released molecules *vs.* time was studied using the following mathematical models:

$$F_t = M_\infty(1 - e^{-k't}) + k_0 t \quad (3)$$

$$F_t = kt^n \quad (4)$$

where $F_t$ is the drug release fraction at time $t$, $k$ is the kinetic release constant of the respective equations, $t$ is the release time and $n$ is the characteristic diffusion exponent, depending on the release mechanism and the geometry of the device. If Fickian diffusion occurred, $n$ decreased to 0.5 for slab/cylinder/sphere. If non-Fickian (anomalous) diffusion dominated, the $n$ value was between the above value corresponding to the polymer chain relaxation ($n < 1$) for a slab/cylinder/sphere. Thus, through determination of the $n$ value, the drug release mechanism could be identified.

### CPT release from the gel matrix

Hybrid gels obtained both in PB and PBS at 0.3 wt% Fmoc-F and 0.1 wt% f-HNT/CPT ([CPT] = $7.29 \times 10^{-5}$ M) were prepared, as discussed above, in a total volume of 5 mL. 5 mL of the gelation solvent was casted on the gel matrix. The release kinetics tests were carried out at 37 °C for 5 days.

At fixed intervals of time (Tables S2–S4, ESI‡), 250 μL of supernatant solution were removed to be spectrophotometrically analysed by controlling the CPT peak at 369 nm and simultaneously refilled with 250 μL of the same solvent, pre-warmed at 37 °C. In this way, alterations of the final concentration of camptothecin in the supernatant solution were minimized. The concentration of CPT was determined with a calibration curve (Fig. S12, ESI‡).[64]

### Cell culture and cell proliferation assays

Human cervical cancer HeLa cells were obtained from American Type Culture Collection (Manassas, VA) and cultured in Roswell Park Memorial Institute (RPMI) 1640 medium supplemented with 10% fetal bovine serum and 2 mM L-glutamine, 100 units per mL penicillin and 100 mg $mL^{-1}$ streptomycin (Gibco Life Technologies) and incubated at 37 °C in 5% $CO_2$. The cells were plated at a density of $1 \times 10^4$ cells per well on 96-well plates and incubated overnight. The cells were then treated with different doses of camptothecin for 24 hours. After treatment, 3-(4,5-dimethylthiazol-2-yl)-5-(3-carboxymethoxyphenyl)-2(4-sulfophenyl)-2*H*-tetrazolium (MTS) was added to the cells and allowed to develop for 1 hour. Colorimetric measurements were performed at 490 nm using an ELISA plate reader.

## Acknowledgements

The authors would thank Dr I. Pibiri (University of Palermo) for the POM measurements and Dr S. Guernelli (University of Bologna) for the TEM investigations. We thank MIUR (FIRB 2010RBFR10BF5V), FIRB 2012 (prot. RBFR12ETL5) for financial support.

## Notes and references

1 G. Parekh, P. Pattekari, C. Joshi, T. Shutava, M. DeCoster, T. Levchenko, V. Torchilin and Y. Lvov, *Int. J. Pharm.*, 2014, **465**, 218.
2 S. Mu, Y. Liang, S. Chen, L. Zhang and T. Liu, *Mater. Sci. Eng., C*, 2015, **50**, 294.
3 S. Xu, H. Fan, L. Yin, J. Zhang, A. Dong, L. Deng and H. Tang, *Eur. J. Pharm. Biopharm.*, 2016, **104**, 251.
4 A. Rivera, L. Valdés, J. Jiménez, I. Pérez, A. Lam, E. Altshuler, L. C. De Ménorval, J. O. Fossum, E. L. Hansen and Z. Rozynek, *Appl. Clay Sci.*, 2016, **124–125**, 150.
5 Y. M. Lvov, M. M. DeVilliers and R. F. Fakhrullin, *Expert Opin. Drug Delivery*, 2016, 1, DOI: 10.1517/17425247.2016.1169271.
6 Y. Lvov, W. Wang, L. Zhang and R. Fakhrullin, *Adv. Mater.*, 2016, **28**, 1227.
7 G. I. Fakhrullina, F. S. Akhatova, Y. M. Lvov and R. F. Fakhrullin, *Environ. Sci.: Nano*, 2015, **2**, 54.
8 M. Kryuchkova, A. Danilushkina, Y. Lvov and R. Fakhrullin, *Environ. Sci.: Nano*, 2016, **3**, 442.
9 L. Bellani, L. Giorgetti, S. Riela, G. Lazzara, A. Scialabba and M. Massaro, *Environ. Toxicol. Chem.*, 2016, **35**, 2503.
10 M. Liu, Z. Jia, D. Jia and C. Zhou, *Prog. Polym. Sci.*, 2014, **39**, 1498.
11 C. Bretti, S. Cataldo, A. Gianguzza, G. Lando, G. Lazzara, A. Pettignano and S. Sammartano, *J. Phys. Chem. C*, 2016, **120**, 7849.
12 F. Arcudi, G. Cavallaro, G. Lazzara, M. Massaro, S. Milioto, R. Noto and S. Riela, *J. Phys. Chem. C*, 2014, **118**, 15095.
13 G. Cavallaro, G. Lazzara and S. Milioto, *J. Phys. Chem. C*, 2012, **116**, 21932.
14 G. Cavallaro, G. Lazzara, S. Milioto, F. Parisi and V. Sanzillo, *ACS Appl. Mater. Interfaces*, 2014, **6**, 606.
15 J. Tully, R. Yendluri and Y. Lvov, *Biomacromolecules*, 2016, **17**, 615.
16 M. Massaro, S. Riela, G. Cavallaro, C. G. Colletti, S. Milioto, R. Noto, F. Parisi and G. Lazzara, *J. Mol. Catal. A: Chem.*, 2015, **408**, 12.
17 M. Massaro, S. Riela, G. Lazzara, M. Gruttadauria, S. Milioto and R. Noto, *Appl. Organomet. Chem.*, 2014, **28**, 234.
18 M. Massaro, V. Schembri, V. Campisciano, G. Cavallaro, G. Lazzara, S. Milioto, R. Noto, F. Parisi and S. Riela, *RSC Adv.*, 2016, **6**, 55312.
19 Y. Fu, D. Zhao, P. Yao, W. Wang, L. Zhang and Y. Lvov, *ACS Appl. Mater. Interfaces*, 2015, **7**, 8156.
20 E. A. Naumenko, I. D. Guryanov, R. Yendluri, Y. M. Lvov and R. F. Fakhrullin, *Nanoscale*, 2016, **8**, 7257.
21 M. Massaro, C. G. Colletti, G. Lazzara, S. Guernelli, R. Noto and S. Riela, *ACS Sustainable Chem. Eng.*, 2017, **5**, 3346.
22 M. Liu, Y. Chang, J. Yang, Y. You, R. He, T. Chen and C. Zhou, *J. Mater. Chem. B*, 2016, **4**, 2253.
23 M. Massaro, R. Amorati, G. Cavallaro, S. Guernelli, G. Lazzara, S. Milioto, R. Noto, P. Poma and S. Riela, *Colloids Surf., B*, 2016, **140**, 505.
24 M. Massaro, S. Piana, C. G. Colletti, R. Noto, S. Riela, C. Baiamonte, C. Giordano, G. Pizzolanti, G. Cavallaro, S. Milioto and G. Lazzara, *J. Mater. Chem. B*, 2015, **3**, 4074.

 

25 M. Massaro, S. Riela, S. Guernelli, F. Parisi, G. Lazzara, A. Baschieri, L. Valgimigli and R. Amorati, *J. Mater. Chem. B*, 2016, **4**, 2229.

26 M. Massaro, G. Lazzara, S. Milioto, R. Noto and S. Riela, *J. Mater. Chem. B*, 2017, DOI: 10.1039/C7TB00316A.

27 M. Massaro, S. Riela, C. Baiamonte, J. L. J. Blanco, C. Giordano, P. Lo Meo, S. Milioto, R. Noto, F. Parisi, G. Pizzolanti and G. Lazzara, *RSC Adv.*, 2016, **6**, 87935.

28 E. A. Appel, J. del Barrio, X. J. Loh and O. A. Scherman, *Chem. Soc. Rev.*, 2012, **41**, 6195.

29 A. P. Constantinou and T. K. Georgiou, *Eur. Polym. J.*, 2016, **78**, 366.

30 F. D'Anna, P. Vitale, S. Marullo and R. Noto, *Langmuir*, 2012, **28**, 10849.

31 X. Du, J. Zhou, J. Shi and B. Xu, *Chem. Rev.*, 2015, **115**, 13165.

32 C. Rizzo, F. D'Anna, S. Marullo, P. Vitale and R. Noto, *Eur. J. Org. Chem.*, 2014, 1013.

33 J. K. Kretsinger, L. A. Haines, B. Ozbas, D. J. Pochan and J. P. Schneider, *Biomaterials*, 2005, **26**, 5177.

34 A. M. Smith, R. J. Williams, C. Tang, P. Coppo, R. F. Collins, M. L. Turner, A. Saiani and R. V. Ulijn, *Adv. Mater.*, 2008, **20**, 37.

35 M. Suzuki, H. Saito and K. Hanabusa, *Langmuir*, 2009, **25**, 8579.

36 D. M. Ryan, S. B. Anderson, F. T. Senguen, R. E. Youngman and B. L. Nilsson, *Soft Matter*, 2010, **6**, 475.

37 Z. Yang, H. Gu, D. Fu, P. Gao, J. K. Lam and B. Xu, *Adv. Mater.*, 2004, **16**, 1440.

38 Z. Yang and B. Xu, *Chem. Commun.*, 2004, 2424, DOI: 10.1039/B408897B.

39 I. Irwansyah, Y.-Q. Li, W. Shi, D. Qi, W. R. Leow, M. B. Y. Tang, S. Li and X. Chen, *Adv. Mater.*, 2015, **27**, 648.

40 S. Raghavan and B. Cipriano, in *Molecular Gels*, ed. R. Weiss and P. Terech, Springer, Netherlands, 2006, ch. 9, p. 241, DOI: 10.1007/1-4020-3689-2_9.

41 S. Riela, M. Massaro, C. G. Colletti, A. Bommarito, C. Giordano, S. Milioto, R. Noto, P. Poma and G. Lazzara, *Int. J. Pharm.*, 2014, **475**, 205.

42 P. Chakraborty, P. Bairi, S. Mondal and A. K. Nandi, *J. Phys. Chem. B*, 2014, **118**, 13969.

43 R. I. Iliescu, E. Andronescu, C. D. Ghitulica, G. Voicu, A. Ficai and M. Hoteteu, *Int. J. Pharm.*, 2014, **463**, 184.

44 G. Cavallaro, G. Lazzara, S. Milioto and F. Parisi, *Langmuir*, 2015, **31**, 7472.

45 G. Cavallaro, G. Lazzara, M. Massaro, S. Milioto, R. Noto, F. Parisi and S. Riela, *J. Phys. Chem. C*, 2015, **119**, 8944.

46 Y. Bae, S. Lee, E. S. Green, J. H. Park, K. S. Ko, J. Han and J. S. Choi, *Int. J. Pharm.*, 2016, **501**, 75.

47 S. Dong, B. Zheng, D. Xu, X. Yan, M. Zhang and F. Huang, *Adv. Mater.*, 2012, **24**, 3191.

48 X. Huang, S. R. Raghavan, P. Terech and R. G. Weiss, *J. Am. Chem. Soc.*, 2006, **128**, 15341.

49 D. J. Adams, K. Morris, L. Chen, L. C. Serpell, J. Bacsa and G. M. Day, *Soft Matter*, 2010, **6**, 4144.

50 L. E. Buerkle and S. J. Rowan, *Chem. Soc. Rev.*, 2012, **41**, 6089.

51 D. V. Malakhov and M. K. Abou Khatwa, *J. Therm. Anal. Calorim.*, 2007, **87**, 595.

52 L. Chiappisi, G. Lazzara, M. Gradzielski and S. Milioto, *Langmuir*, 2012, **28**, 17609.

53 F. D'Anna, C. Rizzo, P. Vitale, G. Lazzara and R. Noto, *Soft Matter*, 2014, **10**, 9281.

54 C. Daniel, C. Dammer and J.-M. Guenet, *Polymer*, 1994, **35**, 4243.

55 A. Garai and A. K. Nandi, *J. Polym. Sci., Part B: Polym. Phys.*, 2008, **46**, 28.

56 I. Rosalina and M. Bhattacharya, *Carbohydr. Polym.*, 2002, **48**, 191.

57 E. Morici, A. Di Bartolo, R. Arrigo and N. T. Dintcheva, *Polym. Bull.*, 2017, **73**, 3385.

58 P. Mukhopadhyay, N. Fujita, A. Takada, T. Kishida, M. Shirakawa and S. Shinkai, *Angew. Chem., Int. Ed.*, 2010, **49**, 6338.

59 Y. Ohsedo, M. Miyamoto, A. Tanaka and H. Watanabe, *New J. Chem.*, 2013, **37**, 2874.

60 Y. Zhang and R. G. Weiss, *J. Colloid Interface Sci.*, 2017, **486**, 359.

61 S.-Y. Qin, M.-Y. Peng, L. Rong, B. Li, S.-B. Wang, S.-X. Cheng, R.-X. Zhuo and X.-Z. Zhang, *Regener. Biomater.*, 2015, **2**, 159.

62 N. M. Franson and N. A. Peppas, *J. Appl. Polym. Sci.*, 1983, **28**, 1299.

63 S. Raghavan and B. Cipriano, in *Molecular Gels*, ed. R. G. Weiss and P. Terech, Springer, Netherlands, 2006.

64 D. Ma, H.-B. Zhang, K. Tu and L.-M. Zhang, *Soft Matter*, 2012, **8**, 3665.